Article

Not peer-reviewed version

N′-((E)-3,3-Diphenyl-2,3-Dihydro-1H-Inden-1-Ylidene)-2-((Z)-2-Oxoindolin-3-Ylidene)Hydrazine-1-Carbothiohydrazide Ligand and Its Complexes: Spectroscopic, Molecular Orbital, Molecular Docking, Structural Study and Antimicrobial Activity

Ehab M Zayed *, Wael A. El-Sayed, Marzough Aziz Albalawi, Hayam A Abd El Salam, Fatma A El-Samahy, Gehad G. Mohamed

Posted Date: 26 October 2023

doi: 10.20944/preprints202310.1652.v1

Keywords: indanone; thio-carbohydrazones; isatin; metals-synthesis-organometallics; computational study; molecular docking; antimicrobial activity

Article

N′-((E)-3,3-Diphenyl-2,3-Dihydro-1H-Inden-1-Ylidene)-2-((Z)-2-Oxoindolin-3-Ylidene)Hydrazine-1-Carbothiohydrazide Ligand and Its Complexes: Spectroscopic, Molecular Orbital, Molecular Docking, Structural Study and Antimicrobial Activity

Ehab M. Zayed [1,*], Wael A. El-Sayed [2,3], Marzough Aziz albalawi [4], Hayam A. Abd El Salam [1], Fatma A. El-Samahy [1] and Gehad G. Mohamed [5,6]

[1] Green Chemistry Department, National Research Centre, 33 El-Bohouth St. (former El Tahrir St.), P.O. 12622, Dokki, Giza, Egypt
[2] Department of Chemistry, College of Science, Qassim University, Buraidah 51452, Saudi Arabia
[3] Photochemistry Department, National Research Centre, Cairo 12622, Egypt
[4] Chemistry Department, Alwajh college, University of tabuk, Saudi Arabia
[5] Chemistry Department, Faculty of Science, Cairo University, Giza 12613, Egypt
[6] Nanoscience Department, Basic and Applied Sciences Institute, Egypt-Japan University of Science and Technology, New Borg El Arab, Alexandria, 21934, Egypt
* Correspondence: ehab_zyed2002@yahoo.com

Abstract: New Schiff base of N′-((E)-3,3-diphenyl-2,3-dihydro-1H-inden-1-ylidene)-2-((Z)-2-oxoindolin-3-ylidene)hydrazine-1-carbothiohydrazide (HL) and its Co(II),Ni(II), Fe(III), Cu(II), Cd(II), Zn(II) and Mn(II) complexes were created, isolated, and characterized by analytical analysis in good yields of 60 to 90%, UV–Vis, magnetic measurements, molar conductivity, and FT-IR. Additionally, mass spectrometry was used to examine the new ligand complexes' structural characteristics.^{1}H NMR spectroscopy and elemental analysis. Depending on the electronic spectra and magnetic susceptibility measurements, these complexes are predicted to have octahedral molecular geometry. As an example, the quantum chemical properties, bond lengths, and bond angles were discussed. The structural formula for the examined ligand was improved using the Gaussian09 tool. The DFT/B3LYP method was used to calculate the energy gaps and other crucial theoretical features. The prepared hydrazine ligand complexes Co (II), Ni (II), Fe (III), Cu (II), Cd (II), Zn (II) and Mn (II) complexes were evaluated for its antimicrobial properties. As antimicrobial agents, it was found that the organic ligand was less biologically active than the targeted complexes. Gram positive bacteria (3ty7-Staphylococcus), Gram negative bacteria (3t88-Escherichia coli), and fungi (5k04-Candida albicans) all have crystal structures that interact well with the chemicals in the title, according to molecular docking.

Keywords: indanone; thio-carbohydrazones; isatin; metals-synthesis-organometallics; computational study; molecular docking; antimicrobial activity

1. Introduction

Due to their extensive variety of therapeutic, chemical, and biological action, Schiff base (CH=N-) molecules represent a prominent class of organic chemistry. As bi-, tri-, tetra-, or multi-dentate ligands, Schiff bases function as chelating agents because they include nitrogen, oxygen, or sulphur [1–4]**.** The indanone derivatives and their structural analogs are widely employed in agriculture, medicine, and the synthesis of natural products. Indanone derivatives have antimicrobial, antibacterial, antiviral, anticancer, vasodilatation, anticonvulsant, anti-diabetic, antimalarial, anti-inflammatory, the treatment of Alzheimer disease, insecticidal [5–7] and activities.

Preprints (www.preprints.org) | NOT PEER-REVIEWED | Posted: 26 October 2023 doi:10.20944/preprints202310.1652.v1

Thio/carbohydrazones are moreover a significant class of synthetic organic chemistry. Pharmaceutical and biological properties like antiviral, anticancer, antituberculosis, antileishmanial, antimicrobial, and antibacterial have been documented for them [8–10]. Thiocarbohydrazone chain has an aromatic ring at the hydrazono end, which is thought to play a role in interactions with biomolecules that change biological activity. The isatin moiety was chosen because to its high acidity as an ionizable centre, which makes metal coordination easier, as well as the fact that it preserved the fundamental configuration of the three donor atoms. Schiff bases based on isatin are highly sought-after as antibacterial substances. The majority of infections that are acquired in hospitals and the general public are caused by Gram-positive and Gram-negative microorganisms [11–15]. The effectiveness of the drugs is declining daily as a result of the incorrect, prolonged, and widespread use of antibiotics, which has serious health consequences. The rise in bacterial resistance in recent years has made it a key priority for scientists to find innovative antibacterial drugs [16–19]. In this paper, new Schiff bases based on 3,3-diphenyl-2,3-dihydro-1H-inden-1-one and (thio)/carbohydrazone were obtained by reaction of 3,3-diphenyl-2,3-dihydro-1H-inden-1-one - β - thiocarbohydrazone with isatin in the presence of glacial acetic acid under reflux in ethanol. FT-IR, 1H NMR, and 13C NMR spectroscopic methods and elemental analysis were used to confirm the structures of all compounds. Gramme positive bacteria (3ty7-Staphylococcus), Gramme negative bacteria (3t88-Escherichia coli), and fungi (5k04-Candida albicans) all responded favorably to the compounds' putative antibacterial properties.

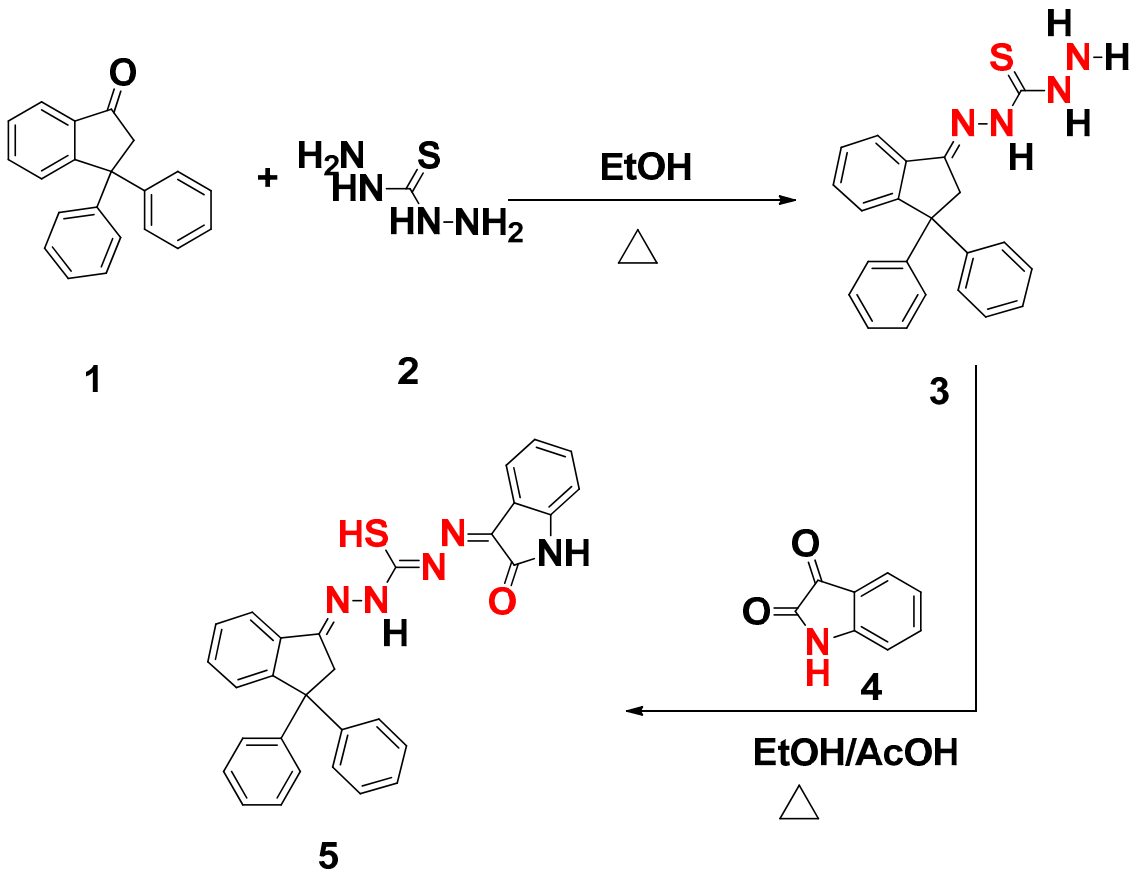

Scheme 1

Scheme 1. preparation of hydrazones ligand.

 doi:10.20944/preprints202310.1652.v1

2. Results and discussion

The complexation of hydrazones ligand was generated from the reaction of metal (II) and metal (III) chlorides with synthesized hydrazones ligand in 1:2 molar ratios. The analytical techniques revealed that synthesized hydrazones ligand was bonded to metal ions *via* the azomethine nitrogen atoms, phenolic oxygen atoms and SH atoms this yields octahedral geometry. To determine the geometry of the complexes and other identifying information, the compounds were analyzed using a variety of spectroscopic and physical approaches (Elemental analyses, X-ray diffraction, UV-Vis, FTIR, and other methods were used to comprehensively characterize each of these complexes), which are in good agreement with the information needed to determine the general composition $[M(H_2L)_2].Cl_2$(where M = Cu(II), Co(II), Ni(II), Fe(III), Zn(II), Mn(II), and Cd(II). The produced complexes are relatively stable in the solid form at room temperature, insoluble in water, methanol, and ethanol, but only soluble in DMF and DMSO. The metal complexes could not be grown into a single crystal, despite numerous attempts. The $[M(H_2L)_2]Cl_2$formulae were indicated by the complexes' molar conductivity values in DMSO.

2.1. ^1H NMR

Proton ^{1}NMR spectra of the synthesized thiocarbohydrazonesderivative and their zinc(II) complexes were detected in DMSO- $d_6$as solvent. For the thiocarbohydrazones ligand **5**, the singlet signal of aliphatic proton CH_2 of indene derivative was detected at δ= 3.84ppm. The amino group of **3,3-diphenyl-2,3-dihydro-1H-inden-1-one - β -thiocarbohydrazone** was not observed atδ= 4.98ppm. Moreover, the NH peak of isatin ring was observed as a singlet at δ=11.79 ppm.The aryl region's aromatic proton multiplet signals were detected between δ= 6.93 and 8.05 ppm with a rise in number of proton by 4H of isatine from compound **3**. This evidence confirmed the expected outcome of the reaction. The peaks of (NH and SH) of thiocarbohydrazone moiety were detected at as singlet at δ= 11.32and 14.73 ppm , respectively and the intensity of this signals decrease on complexation. This guarantees that the -NH proton will decrease as a result of thio carbohydrazone ligands' binding to zinc(II) ions, which is made possible through tautomerization via the thione..The aromatic proton signals of the aryl region were observed between δ 6.93-8.05ppm. ^{13}C NMR spectra of H2L1 ligand show the characteristics signalat δ= 47.2, 59.5 of C2 and C3 of indene. The signal of the aromatic region was detected at δ 111.7-147.7ppm. The C=O signal of isatin at δ= 176.6ppm. The characteristic 3 CH = N peaks were detected at δ= 154.1, 156.1 and 163.2 ppm.

2.2. Molecular modeling

A theoretical tool for molecular modelling as well as the geometrical shape of the hydrazones ligand was created using the Gaussian09 programme. The diazene carbohydrazonothioic acid ligands electronic structure can be determined by looking at the border orbital energy gap between ELUMO and EHOMO [20–23]. According to illustrations of the free diazene carbohydrazonothioic acid ligands molecular orbital's, the donor atoms—nitrogen of hydrazine, sulphur of HS group, and oxygen of OH group—that are employed to donate to metal ion acceptors were predominantly concentrated on the LUMO, HOMO and charge distribution (Figure 1).

Using previously published equations, values for chemical potential (Pi), global softness (S), global electrophilicity index (ω), global hardness (η), absolute softness (S), and electronegativity (χ) values were calculated using previously published equations (Table 1) [24]. The most significant marker of various sites' toxicity and reactivity is. The most important measure, which shows the toxicity and reactivity of various sites, is. Although the recommended diazene ligands are electrophilic, the hydrazones ligand system is picking up extra negative charge from the environment. The reactivity and molecular stability are determined using the parameters and S. The global measures of hardness and softness are at odds with one another [25].

The free hydrazones ligand was revealed to have the following properties following the determination of all the parameters (Table 1). The soft property of the free ligand was used to infer

Preprints (www.preprints.org) | NOT PEER-REVIEWED | Posted: 26 October 2023 doi:10.20944/preprints202310.1652.v1

the flexible reactions to metal ions. The figures show that the chemical can take electrons from its surroundings and lower its energy (Figure 2).

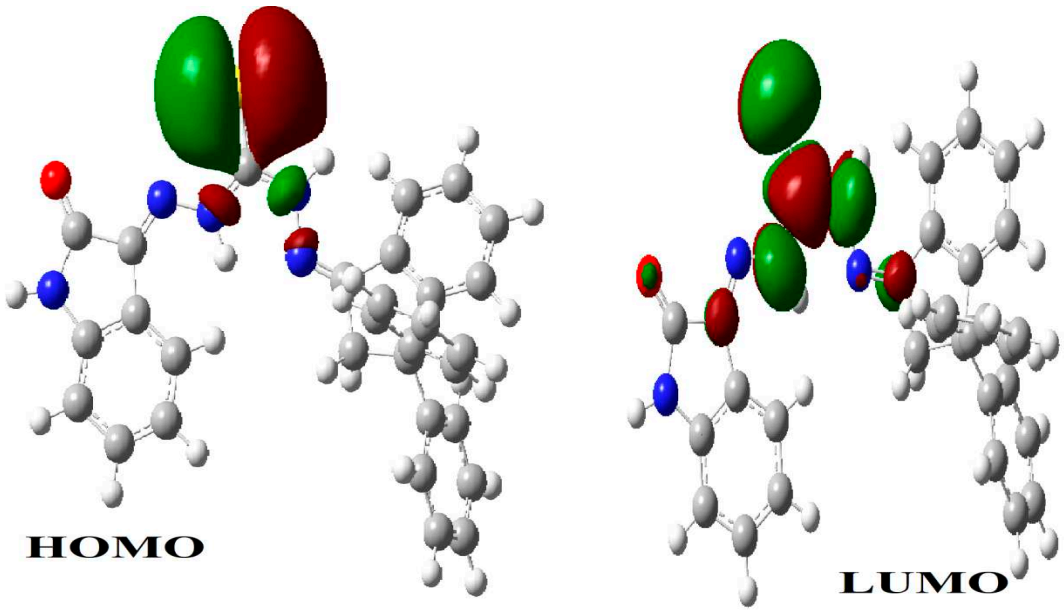

Figure 1. LUMO and HOMO patterns of studied hydrazones ligand.

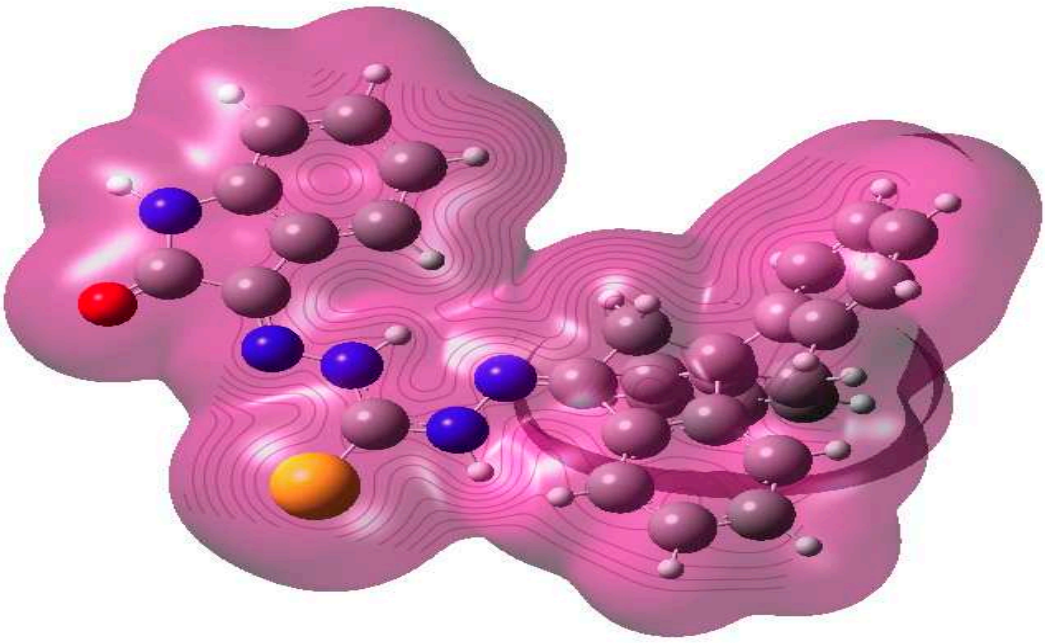

Figure 2. Charge distribution of studied hydrazones ligand.

Table 1. Calculated quantum chemical parameters of hydrazones ligand.

Parameter	eV
E_{HOMO} (eV)	-0.18396
E_{LUMO} (eV)	-0.08354
μ(D)	-3.79687
T.E (eV)	-1893.93
ΔE (eV)	0.10042
χ (eV)	0.13375

Preprints (www.preprints.org) | NOT PEER-REVIEWED | Posted: 26 October 2023 doi:10.20944/preprints202310.1652.v1

η (eV)	0.05021
σ(eV)$^{-1}$	19.91635
Pi (eV)	-0.13375
S (eV)$^{-1}$	9.958176
ω(eV)	0.17814243
ΔN_{max}	2.66381199

2.2.1. Atomic charges, bond lengths and bond angles

Quantum mechanical computation is built on atomic charge calculations [26,27]. With optimised geometry, charges population analysis was used to determine the overall atomic charge, and the results are displayed in the supplemental material (Supplementary Tables S1–S4). The diazene ligand has three promising atoms: nitrogen, oxygen, and sulphur. This shows that the more active site, which promises to produce chelation, is brought on by a high electron density, particularly in the area surrounding hydrazones. The hydrazones ligand structure's numbering scheme was depicted in Figure 3. It can be shown that the melting temperatures of nitrogen, oxygen, and sulphur atoms are greater than those of other atoms of a similar size, indicating that these atoms may be able to form coordination compounds by chelating with metal atoms. The ideal coordination sites of the diazene ligand were predicted using the Mulliken method and molecular electrostatic potential analysis. They all suggest that the link is fragile and that it will be the first to break (Supplementary Tables S1 and S2). This notion was compatible with the outcomes of mass fragmentation and heat deterioration, and it added to the earlier discussion.

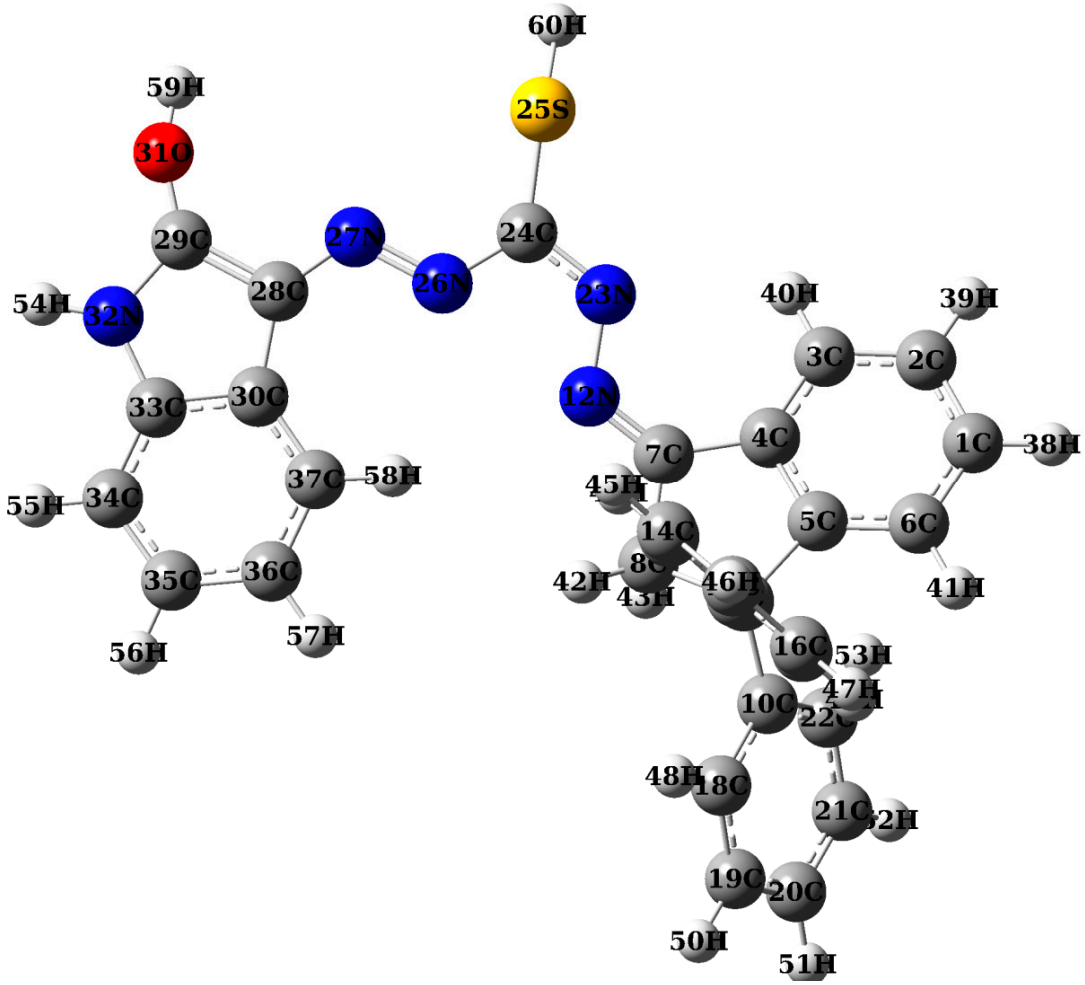

Figure 3. Optimized hydrazones ligand structure with numbering system.

 doi:10.20944/preprints202310.1652.v1

2.3. Characterization of metal complexes

Figure 3 showed the numbering of the hydrazones ligand structure. We can demonstrate that the melting points of nitrogen, oxygen, and sulphur atoms are higher than those of other atoms of a similar size, suggesting that these atoms may be able to chelates with metal atoms to produce coordination compounds. The ideal coordination sites of the diazene ligand were predicted using the Mulliken method and molecular electrostatic potential analysis. All of them (Supplementary Tables S1–S4) show how fragile the relationship is and hint that it will be the first to break. This notion was compatible with the outcomes of mass fragmentation and heat deterioration, and it added to the earlier discussion [28].

2.4. IR spectral studies.

The IR spectrum of hydrazones ligand showed bands at 3176, 1372, 1270, 685, 1239, 1423, 1642, 1481 and 3059 cm^{-1} due to ν(OH), in-plane bending δ(OH), ν(C-O),δ(OH), ν(C=S), ν(C-S), ν(C=N), ν(N=N) and ν(N-H), respectively. The ν(OH), in-plane bending δ(OH), ν(C-O),δ(OH) vibrations in the complexes are shifted to lower frequencies and found at 3129-3213, 1320-1362, 1260-1298 and 653-675 cm^{-1} which indicated that phenolic oxygen was coordinated with metal ions without proton displacement. This positive shift, which shows coordination of the phenolic oxygen [29], may be explained by the drift of oxygen's electron density to the metal ion, which increases the ionic character of the (C-O) bond and raises the frequency of the υ (C-O) vibration. [30].The bands at 1239 and 123 cm^{-1} which can be assigned to ν(C=S) and ν(C-S) of the ligand and it is also shifted to lower wave number after complexation indicating coordination of ligand sulfur atom to metal ions.

The free ν(N=N) is generally observed at ~ 1481cm^{-1}. The observed values are seen to have undergone a positive shift by 3–9 cm^{-1} in all its complexes, due to participation of nitrogen in coordination to metal ions. The free ν(NH) is viewed at 3059 cm^{-1} in the ligand IR spectrum and its shift in metal complexes (3052-3055 cm^{-1}) was due to intermolecular (O-H…..O) or intramolecular hydrogen bonding (OH…..N)/(O-H…O). A medium intensity band at 1642 cm^{-1} in this ligand assignable to υ(C=N) is seen to have undergone a positive shift by 13–25 cm^{-1} in all its complexes, due to change in carbon skeleton of the ligand due to chelates formation and this explain its non participation in coordination.

New bands at 410-426, 448-450, and 510 - 545 cm-1 designated as ν (M-S), (M-N), and (M-O) modes, respectively, further illustrate the coordination of sulphur, nitrogen, and oxygen. The M-O band typically occurs in the higher frequency range and is typically sharper and stronger than the M-N band due to the bigger dipole moment change in the M-O band's vibration compared to that of the M-N band. The emergence of non ligand bands in the range of 960-989 cm-1 that might be attributed to the rocking mode of coordinated water [31–33] further supports the existence of coordinated water. Thermal analysis demonstrated the presence of coordinated water in each of these complexes and presence of lattice water.

2.5. Molar conductivity measurements

Conductivity measurements are used to assess whether counter ions are present inside or outside the coordination sphere. This process was used to gauge how ionized the produced complexes were. When counter ions are present outside of the coordination sphere, the value increases, and vice versa. At room temperature, the molar conductance of the metal complexes in DMF was measured ($1x10^{-3}$ M). The reported conductivity values of 109.2, 105.9, 165.7, 102.2, 106.7, 107.9 and 105.7$Ω^{-1}cm^2mol^{-1}$ for Co(II), Ni(II), Fe(III), Cu(II), Cd(II), Zn(II), and Mn(II) complexes, respectively, may be explained by the fact that the complexes were ionic or electrolytic in nature. All the complexes were electrolytes according to the measured molar conductivity values as the results of the existence of halogens outside the coordination sphere [34].

 doi:10.20944/preprints202310.1652.v1

2.6. Electronic spectra and magnetic moment measurements

Three bands can be seen in the Cu(II) complex: a ligand-metal charge transfer band (21,789 cm^{-1}) and a d-d band (16,740 cm^{-1}). The distorted octahedral geometry of the copper complex is supported by both the magnetic moment value of 1.86 B.M. and the $^{2}E_g \rightarrow {}^{2}T_{2g}$ transition that may be the cause of the d-d band. Three bands identified by the Co(II) complex's electronic spectral data at 24,980, 15,766 and 13,455 cm-1 are assigned to $^{4}T1g(F) \rightarrow {}^{4}T2g(F)$ (ν1),$^{4}T1g(F) \rightarrow {}^{4}A2g(F)$ (ν2), and$^{4}T1g(F) \rightarrow {}^{4}T1g(F)$ (ν3) transitions, respectively suggesting that there is an octahedral geometry around Co(II) ion, which is also supported by its magnetic moment value 4.72B.M.[35]

Three d-d bands are present in the Ni(II) complex at 21,465, 18,634, and 12,324 cm^{-1} as a result of the transitions $^{3}A_{2g}(F) \rightarrow {}^{3}T_{2g}(F)$, $^{3}A_{2g}(F) \rightarrow {}^{3}T_{1g}(F)$, and $^{3}A_{2g}(F) \rightarrow {}^{3}T_{1g}(P)$, respectively. The octahedral geometry of transitions is supported by the magnetic moment value of 3.37B.M.The diffused reflectance spectrum of the paramagnetic (5.53 B.M) Fe(III) complex was ascribed to the four peaks at 22,377, 18,977, 15,699 and 13,640cm^{-1} were assigned to the $^{6}A_1 \rightarrow {}^{4}T_1(G)$, $^{6}A_1 \rightarrow {}^{4}T_2(G)$, $^{6}A_1 \rightarrow {}^{4}A_1, {}^{4}E$ (G), and $^{6}A_1 \rightarrow {}^{4}T_2(D)$transitions, respectively, indicating an octahedral geometry.[36]

Three spin-allowed bands were present in the electronic spectrum of the Mn(II) complex, which correspond to the octahedral geometry at 16,455 $cm^{-1}(^{6}A_{1g} \rightarrow {}^{4}T_{1g}$ (4G)(ν1)], 17,788cm^{-1} ($^{6}A_{1g} \rightarrow {}^{4}T_{2g}$ (G)(ν2)], and 24,768 $cm^{-1}(^{6}A_{1g} \rightarrow {}^{4}E_g$, $^{4}T_{1g} \rightarrow {}^{4}P_g(\nu_3)]$ [16]. Five unpaired electrons are represented by the measured magnetic moment of the Mn(II) complex, which is 5.44 B.M., indicating a high spin octahedral environment.[37]

The d shell is full and not available for bonding in Cd(II) and Zn(II) complexes. Due to the d electrons' absence from metallic bonding, the metal is relatively soft when combined with other transition metals. The full d shell of the Cd(II) and Zn(II) complex ions prevents the stabilizing impact of the ligand field. Therefore, only the factors of size, electrostatic forces, and covalent bonding forces are taken into account when determining the stereochemistry of its complex. Based on the other information presented, octahedral geometry has been suggested for it. [37].

2.7. Mass spectral study

To get the mass spectra of metal complexes, fragmentation was used. In general, significant fragments connected to breakdown products as well as the MS of the ligand and its complexes were obtained. The molecular weight of this ligand is 501.60 g/mol. The peak at 501 m/z in the spectra, which was assigned to [M]+ and confirmed to be a diazene moiety $C_{30}H_{23}N_5OS$, was present. The complexes moieties $C_{60}H_{46}Cl_2CoN_{10}O_2S_2$, $C_{60}H_{46}Cl_2NiN_{10}O_2S_2$, $C_{60}H_{46}Cl_3FeN_{10}O_2S_2$, $C_{60}H_{46}Cl_2CuN_{10}O_2S_2$, $C_{60}H_{46}Cl_2CdN_{10}O_2S_2$, $C_{60}H_{46}Cl_2ZnN_{10}O_2S_2$and $C_{60}H_{46}Cl_2MnN_{10}O_2S_2$had a peak at m/z (amu) 1130 (1131.20 g/mol), 1129 (1130.20 g/mol), 1163 (1163.17 g/mol), 1136 (1135.19 g/mol), 1187 (1186.17 g/mol), 1135 (1136.19 g/mol) and 1128 (1127.20 g/mol) which, in turn, corresponds to the complex moieties in the spectra of the relevant complexes of Co(II), Ni(II), Fe(III), Cu(II), Cd(II), Zn(II), and Mn(II). A peak at m/z 501, 350, 301, 235, 160, 133, and 78, respectively, indicated the ligand moiety. In Scheme 2, fragmentation paths and piece structural assignments are suggested.

Preprints (www.preprints.org) | NOT PEER-REVIEWED | Posted: 26 October 2023 doi:10.20944/preprints202310.1652.v1

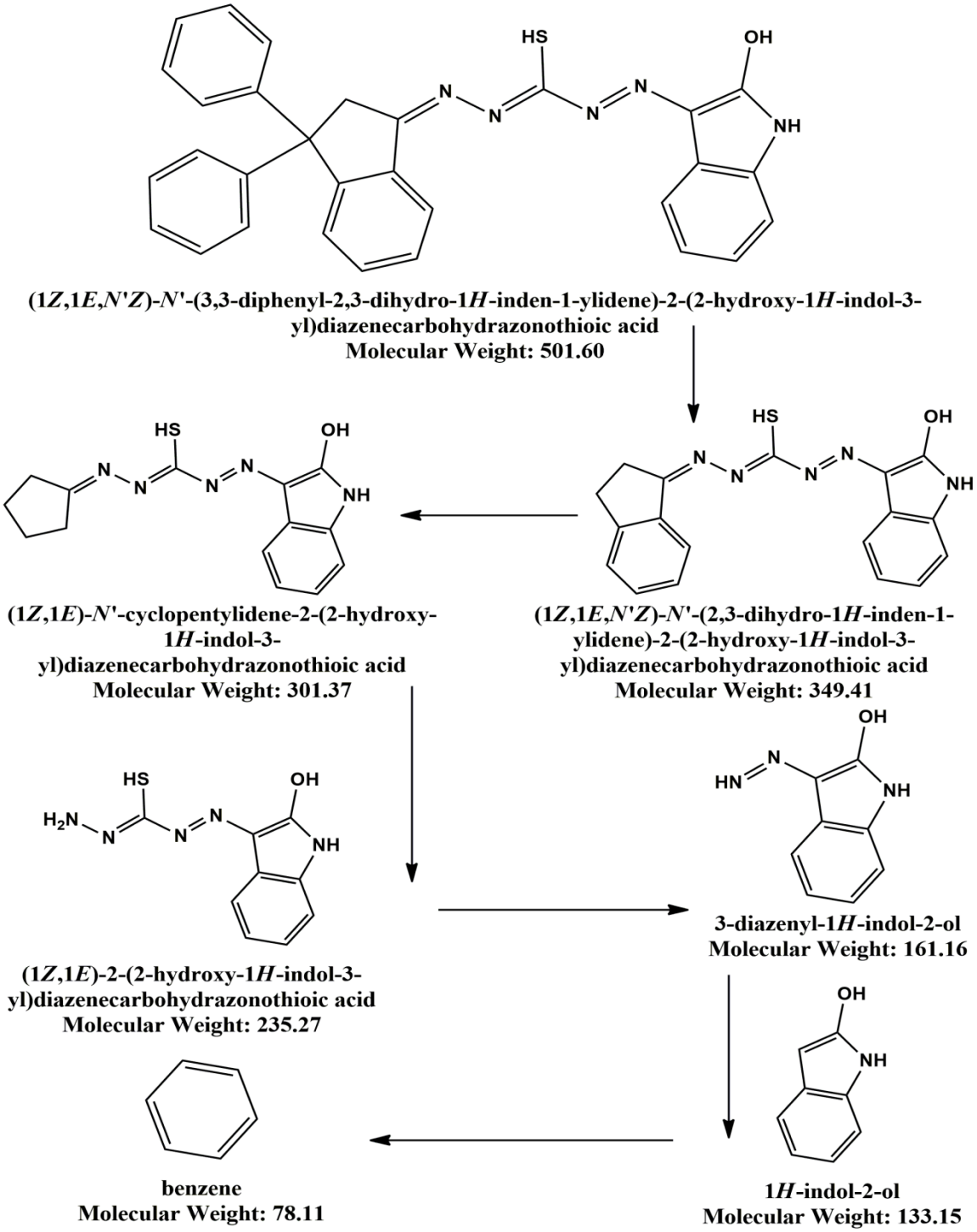

Scheme 2. Mass and suggested fragmentation for hydrazones ligand.

2.8. Thermogravimetric analysis data

The weight loss percentages of the H_2L hydrazones ligand and its complexes of Co(II), Ni(II), Fe(III),Cu(II),Zn(II),Cd(II) and Mn(II) in the temperature range of 40–800 °C were studied.

The TGA curve of hydrazones ligand (H_2L) showed decomposition peak at 50 °C in three stages. Weight loss percentage of the first step at the temperature range 40 -400 °C found 15.56% (calcd. 15.82%) due to loss of C_6H_6. The second stage is found loss of$C_9H_7N_2S$ (found 33.93%; calcd. 34.51%) (150-250°C). The final stage at the temperature range 250-400 °C due to loss of $C_{15}H_{10}N_3O$ (found 35.61%;calcd. 48.86%).The overall approximate weight loss was found to be 97.99%, and the percentage of the residue that polluted with carbon was determined after that. (calcd. 99.19%).The thermogram data of complexes show multiple TGA stages of degradation. Co (II) Complex gave four

Preprints (www.preprints.org) | NOT PEER-REVIEWED | Posted: 26 October 2023 doi:10.20944/preprints202310.1652.v1

stages of degradation through temperature range 50-1000 °C, first stage from temperature range 50-150 °C, which is convenient to lose C_2H_2,H_2O and 2HCl (found 6.87%; calc. 7.16%), the second stage start from temperature 150-250 °C, with lose of $C_{12}H_{10}N_5S$ molecules (found 22.31%; calc. 22.63%), the lose molecules in third one , $C_{33}H_{20}N_5S$ at temperature range 250-600, with (found 44.98%; calc. 45.80) percent, the last stage lay in temperature 600-1000°C, lose molecules ; $C_{13}H_{10}$ with lose percent (found 18.15%; calc 17.78%), The overall approximate weight loss was found to be 92.31%, and the percentage of the residue that is Co (II) oxide polluted with carbon was determined after that. (calcd. 93.37%).

Ni(II) Complex gave the first stage of degradation in range40-160 °C due to lose of molecules; 2HCl, H_2O and C_3H_5, with percent (found 11.45%; calc 11.76%).Also, decomposed at the range 160-280 °C in the second stage losing $C_{21}H_{17}N_5S$ (found 32.76%; calc. 33.27%),in step three with temperature range 280-650°C, we notice lose of $C_{18}H_{11}N_3S$ molecule (found 26.31%; calc 26.90%), the last stage lay in temperature 650-1000°C, lose molecules ; $C_{18}H_9N_2$ with lose percent (found 20.87%; calc 21.53%), The overall approximate weight loss was found to be 91.39%, and the percentage of the residue that is Ni(II) oxide polluted with carbon was determined after that. (calcd. 93.46%) Table 2.

while the Fe(III) and Cu(II) complexes degraded in four stages; the first at temperature ranges 50-280 °C and 40-250°C, due to the loss of3HCl and C_9H_{10}(found 20.32%; calc. 19.69%) and H_2O, 2HCl and C_5H_4(found 12.66%; calc. 13.72%)moieties , respectively. Also, in second step at temperature ranges 280-570 °C and 250-560°C due to the leave of $C_{18}H_{12}N_5$ S molecule (found 28.64%; calc. 28.80%) and $C_{24}H_{15}N_5S$ (found 35.72%; calc. 36.05%)respectively. The third one; the molecule leave,($C_{24}H_{13}N_5S$, and 1/2 O) and $C_{23}H_{12}N_4S$respectively, at temperature range 570-800°C and 560-750°Crespectively, with percent (found 35.72%; calc. 35.76%) and (found 33.81%; calc. 33.42%)respectively. The approximate total weight loss was determined to be 93.13 and 93.06, and the residue percentage of the residue that is Fe(III) oxide and Cu(II) oxide were polluted with carbon was determined after that. (calcd. 94.22% and 93.91%) respectively Table 2.

The last three complexes; Cd(II) , Zn(II) and Mn(II) gave three decomposition region, the first stage due to the loss of 2HCL, H_2O and $C_{13}H_{11}$, 2HCl, H2O and $C_{16}H_{10}$ and 2 HCl, H_2O and $C_{14}H_{12}$ molecules respectively. At temperature ranges 150-550 °C, 140-570°C and 180-580 °C, with correspond percent loss (found 21.35%; calc. 21.83%) , (found 25.13%; calc. 25.88%) and (found 24.63%; calc. 24.13%) respectively. The second decomposition step at temperature range 550-800°C, 570-750°C and 580-860 °C respectively, by leaving molecules; $C_{31}H_{20}N_6S_2$, $C_{22}H_{11}N_7S$ and $C_{23}H_{20}N_6S$respectively, with percent lose ; (found 45.67%; calc. 46.03%) , (found 35.45%; calc. 36.26%) and (found 36.89%; calc. 37.08%) respectively. The last stage laying in temperature range; 800-1000 °C, 750-1000 and 860-1000 °C, with leaving groups; $C_{16}H_{11}N_4$, $C_{22}H_{21}N_3S$ and $C_{23}H_{10}N_4S$, the loss percent; (found 22.19%; calc. 22.17%) , (found 32.29%; calc. 31.86%) and (found 32.19%; calc. 33.54%) respectively. The overall approximate weight loss was found to be 89.21%, 92.87% and 91.10, and the percentage of the residue that is Cd(II) oxide, Zn(II) oxide and Mn(II) oxide were polluted with carbon was determined after that. (calcd. 90.03%, 94.00% and 91.32%) respectively Table 2.

Table 2. Thermo analytical results (TG, DTG) for **hydrazones** ligand and metal complexes.

Compound	TG range (°C)	DTG_{max} (°C)	n*	Mass Loss Total mass Loss Calcd (Estim) %	Assignment	residue
H_2L	40–150	75	1	15.82 (15.56)	- Loss of C_6H_6	--------
	150-250	200	1	34.51 (33.93) 99.19 (97.99)	- Loss of $C_9H_7N_2S$	
	250-400	300	1	48.86 (35.61)	-Loss of $C_{15}H_{10}N_3O$	
$[Co(H_2L)_2].Cl_2$	50-150	110	1	7.16 (6.87)	- Loss of 2HCl, H_2O and C_2H_2.	CoO
	150-250	200	1	22.63 (22.31)93.37 (92.31)	- Loss of$C_{12}H_{10}N_5S$.	
	250-600	400	1	45.80 (44.98)	- Loss of $C_{33}H_{20}N_5S$	
	600-1000	800		17.78 (18.15)	- Loss of $C_{13}H_{10}$	
$[Ni(H_2L)_2].Cl_2$	40-160	110	1	11.76. (11.45)	- Loss of 2HCl, H_2O and C_3H_5.	NiO
	160-280	220	1	33.27 (32.76)		

Preprints (www.preprints.org) | NOT PEER-REVIEWED | Posted: 26 October 2023 doi:10.20944/preprints202310.1652.v1

	280-650 650-1000	480 800	1 1	26.90 (26.31)93.46 (91.39) 21.53 (20.87)	- Loss of $C_{21}H_{17}N_5S$ - Loss of $C_{18}H_{11}N_3S$. - Loss of $C_{18}H_9N_2$	
$[Fe(H_2L)_2].Cl_3$	50-280 280-570 570-800 800-1000	160 320 600 850	1 1 1 1	19.69 (20.32) 28.80 (28.64) 35.76 (35.72)94.22 (93.13) 9.97 (8.45)	- Loss of 3HCl and C_9H_{10}. - Loss of $C_{18}H_{12}N_5$ S. - Loss of $C_{24}H_{13}N_5S$ and 1/2 O. - Loss of C_9H_8.	$½Fe_2O_3$
$[Cu(H_2L)_2].Cl_2$	40-250 250-560 560-750 750-1000	170 350 660 880	1 1 1 1	13.72 (12.66) 36.05 (35.72) 33.42 (33.81) 93.91 (93.06) 10.72 (10.84)	- Loss of H_2O, 2HCl and C_5H_4. - Loss of $C_{24}H_{15}N_5S$. - Loss of $C_{23}H_{12}N_4S$. - Loss of $C_8H_{11}N$	CuO

2.9. SEM analysis

The surface morphology of the hydrazones ligands and the related metal complexes were examined using SEM analysis. The Cu(II) and Fe(III) complex and hydrazones ligand have a distinct visual appearance in the SEM image (Figure 4) due to the crystal aggregate that builds up on the thin films and is caused by the minimal fluctuation in the ligand and metals complex particle size and shape. SEM images provide the ligand had an irregular texture and little rock-like bits, whereas metal complexes have a rock-like appearance because the ligand harmonises with the metal ions and closes the gap on the outer surface. The ligands surface morphology is completely different from the surface morphology of metal complexes, which clearly shows the ligands binding to metal ions. [38].

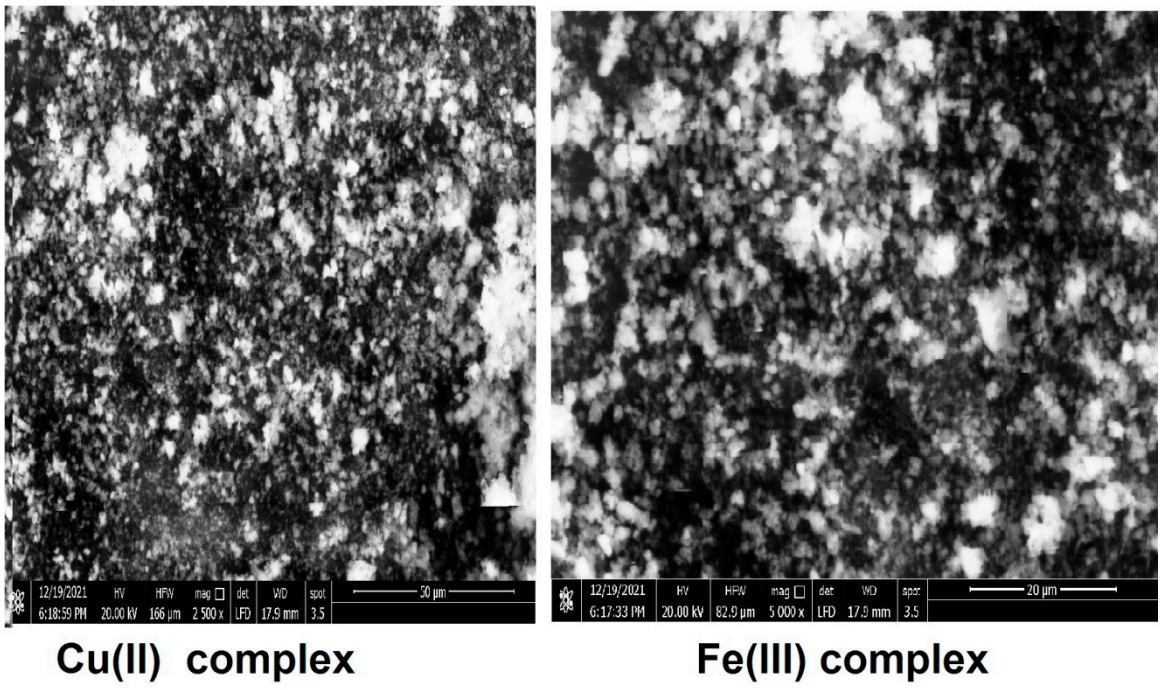

Figure 4. SEM images of (a) Cu (II) complex and (b) Fe(III) complex.

2.10. Molecular Docking

With auto Dock, you can see test results up close and discuss and demonstrate the biological benefits of ligands. G^+ bacteria (3ty7-Staphylococcus), G^- bacteria (3t88-Escherichia coli), and Fungi (5k04 - Candida albicans) are examples of host organisms that can be used to attach ligands (guests). Figures 5–7 shown that HB plots can exhibit a high interaction with all receptors and produce results

Preprints (www.preprints.org) | NOT PEER-REVIEWED | Posted: 26 October 2023 doi:10.20944/preprints202310.1652.v1

that are comparable. All proteins have easily observable inter-hydrogen bonds, calculations showed. To visualize the interactions between docking molecules, two- and three-dimensional images can be used. Using two- and three-dimensional graphics, the mechanism of interaction within docking molecules may be demonstrated. (Figures 5–7).

The interaction between the ligand and the amino acids of the protein was shown to be mostly mediated in the following G^+ bacteria by hydrogen bonding.

For Gram positive bacteria (3ty7-Staphylococcus), An amino acid in the protein reacted with the ligand to cause the H-bond reaction:3ty7-correct-A-h//A/MET`106/OD1– with H bond length 3.3 Aº, 3ty7-correct-A-h//A/GLU`432/O– with hydrogen bond length 2.4 Aº, 3ty7-correct-A-h//A/TYR`410/OD2– with hydrogen bond length 3.4 Aº, 3ty7-correct-A-h//A/THR`280/OD2– with H bond length 3.3 Aº, 3ty7-correct-A-h//A/CYS`279/O– with hydrogen bond length 2.1 Aº, 3ty7-correct-A-h//A/PHR`148/OD2– with H bond length 3.2 Aº and 3ty7-correct-A-h//A/VAL`278/OD2– with H bond length 2.7 Aº, with binding energy = −6.2 kcal mol^{-1}(Figures 5–7).

For Gram negative bacteria (3t88 -Escherichia Coli): amino acid of protein reacted with ligand by H-bond:3t88-correct-A-h/A1/A/ASP`163/OG– with hydrogen bond length 3.2 Aº, 3t88-correct-A-h/A1/A/TYR`97/O– with H bond length 3.3 Aº, 3t88-correct-A-h/A1/A/PHE`162/HZ1– with hydrogen bond length 2.2 Aº, 3t88-correct-A-h/A1/A/ARG`162/O– with H bond length 3.1 Aº and 3t88-correct-A-h/A1/A/LEU`89/HZ1– with hydrogen bond length 2.7 Aº, with binding energy = − 7.3 kcal mol^{-1}(Figures 5–7).

for Fungi (5k04- Candida albicans): amino acid of protein reacted with ligand by H-bond:5k04-h/5k04/B/PRO`50/OH– with hydrogen bond length 2.9 Aº, 5k04-h/5k04/A/LYS`548/O– with H bond length 3.3 Aº, 5k04-h/5k04/A/ASN`552/HN– with hydrogen bond length 2.3 Aº, 5k04-h/5k04/B/GLN`53/OH– with hydrogen bond length 2.1 Aº, 5k04-h/5k04/A/GLY`553/O– with hydrogen bond length 3.5 Aº, 5k04-h/5k04/A/LEU`554/HN– with hydrogen bond length 2.7 Aº, with binding energy = − 10.8 kcal mol^{-1}(Figures 5–7).

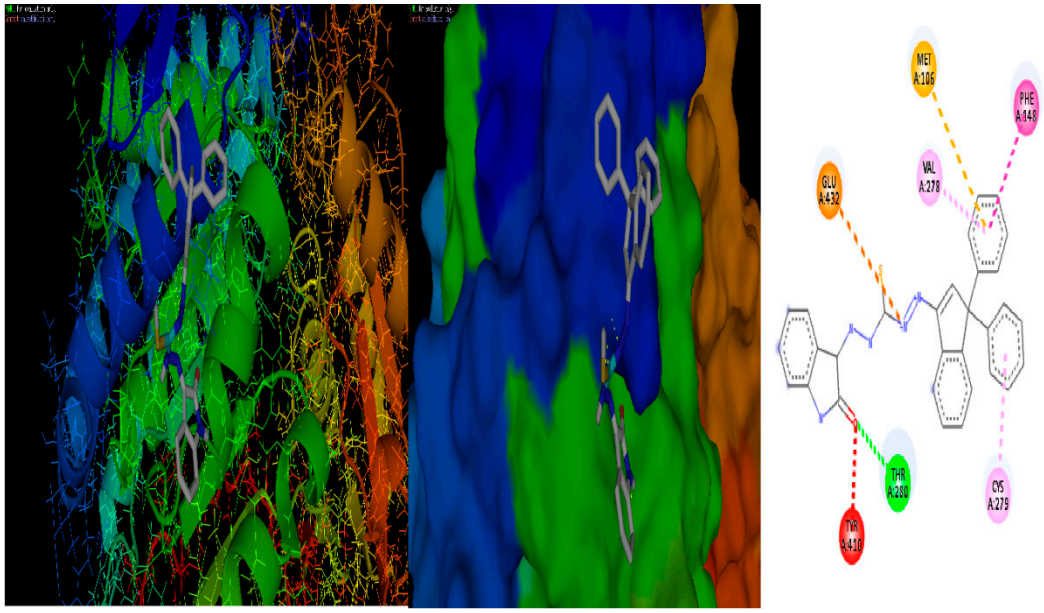

Figure 5. Three-dimensional plot of interaction of hydrazonesligand with *Gram positive bacteria (3ty7-Staphylococcus.*

Preprints (www.preprints.org) | NOT PEER-REVIEWED | Posted: 26 October 2023 doi:10.20944/preprints202310.1652.v1

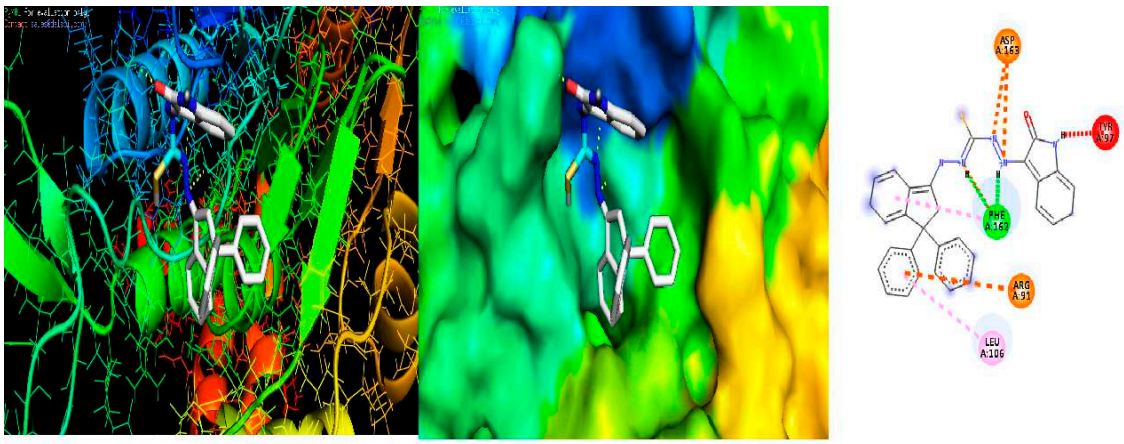

Figure 6. Three-dimensional plot of interaction of hydrazones ligand with Gram negative bacteria (3t88 -Escherichia Coli) receptor.

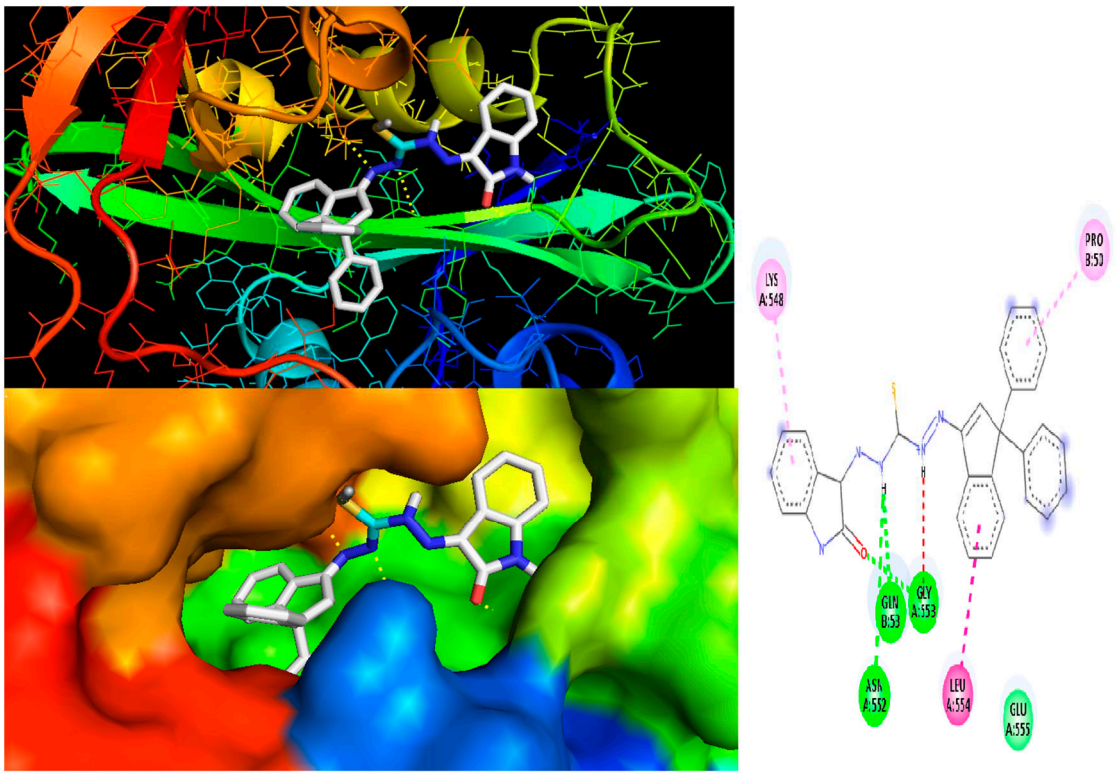

Figure 7. Three-dimensional plot of interaction of hydrazones ligand with Fungi (5k04- Candida albicans) receptor.

2.11. Antimicrobial activity of hydrazones ligand and its metal complexes

Hydrazone ligands' in vitro antibacterial efficacy against a few bacteria and fungi has been assessed. According to the current study, the heteroatom group's chelating properties, the overlap of the metal ion and ligand with donor groups, and the complexes' passage through lipid membranes of cells to inhibit microbial enzymes are all attributed to this activity. The presence of organic bulks also contributes to this activity [39]. In this research, we applied the hydrazones ligands to some species of bacteria like *Streptococcus mutans, Staphylococcus aureus* as G^+ bacteria *Escherichia coli, Klebsiellapneumoniae* and *Pseudomonas sp.* as G^- bacteria and some species of fungi as *Aspergillus niger*and *Candida albicans* as **Fungi** and the results were shown in Figure 8. The results indicated that the hydrazones ligands (H2L) has low antibacterial activity; against **G^+** bacteria; Escherichia coli:10.4 mm, Klebsiella pneumonia:15.6mm and Pseudomonas aeruginosa:13.8mm. And **Gram positive**

Preprints (www.preprints.org) | NOT PEER-REVIEWED | Posted: 26 October 2023 doi:10.20944/preprints202310.1652.v1

bacteria; Staphylococcus aureus:10.5 and Streptococcus mutans:9.82mm[40].For Fungi; Candida albicans:11.8 mm and Asperagillus Nigar:12.8 mm. Where the complexes are varied in activity as follow; for high active complexes as Co(II) and Ni(II) complex; **Gram negative bacteria**: ***Escherichia coli is***33.2 mm and 35.5 mm respectively ,*Klebsiella pneumonia is* 28.1 mm and 27.9 mm respectively, *Pseudomonas aeruginosa:* 34.3 mm and 32.8 mm respectively. Some complexes have moderated activity like: Cu(II), Fe(III) and Mn(II), first display with **Gram negative bacteria,** has three organisms; ***Escherichia coli***30.8 mm, 22.5 mm, 19 mm, respectively, ***Klebsiella pneumonia*** *26*.4 mm, 23.8 mm and 25.7mmrespectively,***Pseudomonas aeruginosa***28.6 mm, 26.3 mm and 27.7 mm, respectively [41–43]. Second display with **Gram positive bacteria,** has tow organisms, ***Staphylococcus aureus***22.1 mm, 28.7 mm, 23.8 mm ,respectively, ***Streptococcus mutans***29.3 mm, 27.9 mm and 22.8 mm, respectively, for fungi, three are tow organisms; ***Candida albicans***27.5 mm , 25.4 mm and 19.7 mm, respectively, ***Asperagillus Nigar*** 21.6 mm, 15.8 mm and 18.9 mm, respectively. the results were shown in Figure 8. Cd(II) complex consider as weak active one as follow; **Gram negative bacteria,** as ***Escherichia coli***12.3 mm, *Klebsiella pneumonia*18.7mm *and Pseudomonas aeruginosa*12.3 mm. **Gram positive bacteria;** *Staphylococcus aureus*17.1 mm and *Streptococcus mutans*14.7 mm. For **Fungi,** firstly; *Candida albicans*15 mm, finally with *Asperagillus Nigar*15.7 mm.

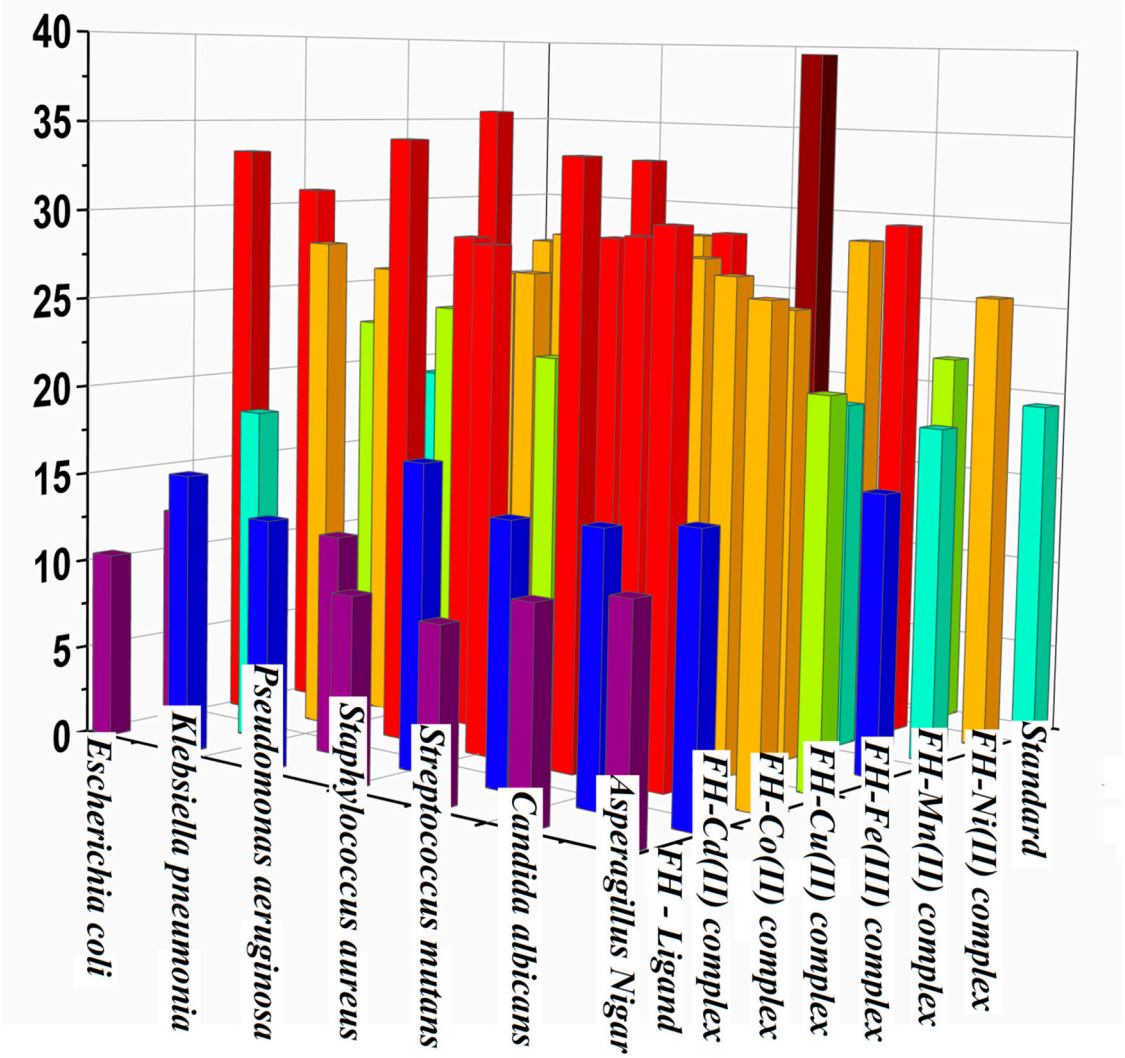

Figure 8. Biological activities of hydrazones ligand and metal complexes.

3. Experimental

The earlier work covered every detail in the experimental portion. [44].

Preprints (www.preprints.org) | NOT PEER-REVIEWED | Posted: 26 October 2023 doi:10.20944/preprints202310.1652.v1

3.1. Materials and reagents

All of the chemicals utilized were of the purest and analytical reagent grade (AR). Sigma-Aldrich provided the chemicals utilized, which included CoCl2.6H2O (BDH), NiCl2.6H2O (BDH), CuCl2.2H2O (BDH), MnCl2.2H2O (BDH), CdCl2.2H2O (BDH), and ZnCl2.2H2O (BDH) m while FeCl3.6H2O was supplied from Prolabo. EtOH and DMF, two organic solvents, were utilized directly out of the package.

3.2. Solutions

A precisely weighed quantity of the prepared metal complex was dissolved in ethanol and DMF (1:3 v/v ratio) to produce a $1x10^{-3}$M solution. A solution of the ligand and its metal complexes ($5 x 10^{-4}$ M) was made for analyzing their UV-Vis spectra by diluting the previously produced stock solutions.

3.3. Synthesis of new Schiff bases based on 3, 3-diphenyl-2,3-dihydro-1H-inden-1-one and thiocarbohydrazone derivatives ligand

3.3.1. Synthesis of 3, 3-diphenyl-2, 3-dihydro-1H-inden-1-one - β -thiocarbohydrazone 3:

A mixture of 3, 3-diphenyl-2, 3-dihydro-1H-inden-1-one (1), thiocarbohydrazide (2) (5 mmol) and glacial acetic acid (10 mL) was heated in absolute ethanol (20 mL) for 3 h. After cooling the mixture, the precipitate that had developed was filtered and cleaned with ethanol (96%) to give compounds **3**.

Yield: 82%. M.p.: °C. FT-IR (KBr, cm-1) υ:3365(NH_2), 3156 (NH), 3019 (CH_2 AL),1670 (C=N), 1596,1504,1490 (C=C), 1323 (C=S) cm^{-1},1H NMR (500 MHz, DMSO-d_6): δ = 3.70 (s,2H,CH_2), 4.98 (s, 2H, NH_2 exchangeable with D_2O), 7.07-7.36 (m,13 H, Ar H), 8.05-8.06 (d,1H, d, J= 7.15 Hz, ArH8-indanine), 9.83 (s,1H,NH exchangeable with D_2O), 10.48 (s,1H,NH exchangeable with D_2O) ppm; 13CNMR (250 MHz, DMSO-d_6): δ = 46.9 (CH_2), 59.2 (C3-indene),123.1, 126.9, 127.4, 128.1, 128.3, 128.9, 131.0, 137.7, 147.9 (18***C***),153.2, 153.7 (2C=N), 177.1(C=S) ppm. MS (EI, m/z): 375(M^{+3}). Anal.Calcd. for $C_{22}H_{20}N_4S$; C, 70.94; H, 5.41; N, 15.04; S, 8.61, found; C, 70.85; H, 5.29; N, 14.32; S, 8.48.

3.3.2. N′-((E)-3,3-diphenyl-2,3-dihydro-1H-inden-1-ylidene)-2-((Z)-2-oxoindolin-3-ylidene)hydrazine-1-carbothiohydrazide 5:

The compound 3,3-diphenyl-2,3-dihydro-1H-inden-1-one-*β*-thiocarbohydrazone(**3)** (2mmol), isatin (2mmol) and glacial acetic acid (3 mL) were heated in absolute ethanol (5 mL) for 5h. The color precipitate created was filtered and cleaned with ethanol (96%) to afford compound (**5**).

FT-IR (KBr, cm-1) υ:3687 (NH isatin ring), 3230 (NH of thiocarbohydrazone), 2824 (CH_2 AL),1692 (CO) isatin ring, 1622 (C=N), 1599,1522,1481 (C=C) cm^{-1}, 1H NMR (500 MHz, DMSO-d_6): δ= 3.84 (s,2H,CH_2), 6.93-8.05 (m,18 H, Ar H),11.32 (s,1H,NH exchangeable with D_2O), 11.79(s,1H,NH exchangeable with D_2O), 14.73 (s,1H,SH exchangeable with D_2O)ppm; 13CNMR (250 MHz, DMSO-d_6):δ =(47.2)C2 of indene, (59.5)C3 of indene, 111.7, 120.7, 121.3, 121.4, 122.5, 123.1, 127.0, 127.5, 127.7, 128.2, 128.7, 128.9, 131.9, 137.2, 138.3, 142.7, 147.7(24 aromatic C), 154.1, 156.1,163.2 (3C=N), C=O (176.6.2)ppm.MS (EI, m/z): 503 (M^{+2}). Anal.Calcd. for $C_{30}H_{23}N_5OS$ C, 71.83; H, 4.62; N, 13.96; S, 6.39; found; C;70.95, H; 4.48; 13.83, S; 6.31%

3.4. Synthesis of metal complexes

The Co(II), Ni(II), Cu(II), Cd(II), Zn(II), Fe(III)and Mn(II) complexes were made by mixing equal amounts(0.119 mmol) of hydrazones ligand with the same metal chloride ratio(lM : 2L molar ratio)in ethanol under refluxed for three hours. Following filtering, the resulting precipitates were collected and repeatedly washed with hot ethanol to produce 88, 85, 89, 79, 88 , 90and 86 percent yield of Co(II), Ni(II), Fe(III), Cu(II), Cd(II), Zn(II) and Mn(II) complexes, respectively. The appropriate products were then dried in a desiccator over anhydrous CaCl2.

Preprints (www.preprints.org) | NOT PEER-REVIEWED | Posted: 26 October 2023 doi:10.20944/preprints202310.1652.v1

$[Co(H_2L)_2(H_2O)_2].Cl_2$; yield 88%; m.p. 280 °C; light blue solid. Anal. Calc. for $C_{60}H_{46}Cl_2CoN_{10}O_2S_2$(%):C, 63.60; H, 4.09; N, 12.36;Cl, 6.26; S, 5.66; M, 5.20. Found (%): C, 63.54; H, 3.95; N, 12.30; Cl, 6.22; S, 5.61; M, 5.15. FT-IR (KBr, ν(OH); 3133m, δ(OH); 1360m, 685m, ν(C-O); 1260m, ν(C=S); 1235m, ν(C-S); 1443m, ν(N=N);1492m, ν(C=N); 1619sh, ν(N-H); 3055s, ν(M-O); 545w, ν(M-N); 448w, ν(M-S);426w.μ_{eff} (BM) 4.66; Λ_m (Ω^{-1} mol^{-1} cm^2) 109.2.

$[Ni(H_2L)_2(H_2O)_2].Cl_2$; yield 85%; m.p.305°C; dark brown solid. Anal. Calc. for $C_{60}H_{46}Cl_2NiN_{10}O_2S_2$(%): C, 63.66; H, 4.14; N, 12.41; Cl, 6.32; S,5.72, M, 5.23.Found (%): C, 63.62; H, 4.09; N,12.36;Cl, 6.26; S, 5.66;M, 5.18. FT-IR (KBr, ν(OH); 3213m, δ(OH); 1353m, 675m, ν(C-O); 1289m, ν(C=S); 1229m, ν(C-S); 1444m, ν(N=N);1493m, ν(C=N); 1619sh, ν(N-H); 3055s, ν(M-O); 520w, ν(M-N); 450w, ν(M-S);423w. μ_{eff} (BM) 2.79; Λ_m (Ω^{-1} mol^{-1} cm^2) 105.9.

$[Cu(H_2L)_2(H_2O)_2].Cl_2$; yield 90%; m.p.300°C; brown solid. Anal. Calc. for $C_{60}H_{46}Cl_2CuN_{10}O_2S_2$(%): C,63.39; H, 4.14; N, 12.36; Cl, 6.27; S, 5.69, M, 5.64. Found (%): C, 63.34; H, 4.08; N,12.31;Cl, 6.23; S, 5.64; M, 5.59. FT-IR (KBr, ν(OH); 3342m, δ(OH); 1326m, 653m, ν(C-O); 1290m, ν(C=S); 1235m, ν(C-S); 1445m, ν(N=N);1492m, ν(C=N); 1617sh, ν(N-H); 3053s, ν(M-O); 510w, ν(M-N); 449w, ν(M-S);414w. μ_{eff} (BM) 1.52; Λ_m (Ω^{-1} mol^{-1} cm^2) 102.2.

$[Fe(H_2L)_2H_2O)_2].Cl_3$; yield 89%; m.p. 287 °C; dark green solid. Anal. Calc. for $C_{60}H_{46}Cl_3FeN_{10}O_2S_2$(%): C, 61.89; H, 4.03; N; 12.08, Cl, 9.17; S, 5.55; M, 4.48. Found (%): C, 61.84; H, 3.98; N; 12.02, Cl, 9.13; S, 5.50; M, 4.79. FT-IR (KBr, ν(OH); 3131m, δ(OH); 1362m, 667m, ν(C-O); 1260m, ν(C=S); 1235m, ν(C-S); 1444m, ν(N=N);1492m, ν(C=N); 1629sh, ν(N-H); 3052s, ν(M-O); 545w, ν(M-N); 448w, ν(M-S);413w. μ_{eff} (BM) 5.83; Λ_m (Ω^{-1} mol^{-1} cm^2) 165.7.

$[Zn(H_2L)_2(H_2O)_2].Cl_2$; yield 79%; m.p.285 °C; light blue solid. Anal. Calc. for$C_{60}H_{46}Cl_2ZnN_{10}O_2S_2$(%): C, 63.29; H, 4.12; N; 12.34;Cl, 6.27; S, 5.68; M, 5.82. Found (%): C, 63.24; H, 4.07; N; 12.29; Cl, 6.22; S, 5.63; M, 5.74. FT-IR (KBr, ν(OH); 3137m, δ(OH); 1362m, 667m, ν(C-O); 1298m, ν(C=S); 1235m, ν(C-S); 1459m, ν(N=N);1484m, ν(C=N); 1626sh, ν(N-H); 3052s, ν(M-O); 544w, ν(M-N); 448w, ν(M-S);410w. μ_{eff} (BM) Diam; Λ_m (Ω^{-1} mol^{-1} cm^2) 107.9.

$[Cd(H_2L)_2(H_2O)_2].Cl_2$;yield 88%; m.p.280 °C; light green solid. Anal. Calc. for $C_{60}H_{46}Cl_2CdN_{10}O_2S_2$(%): C, 30.81; H, 4.32; N, 11.93; Cl, 6.02; S, 5.45; M, 9.52. Found (%): C, 30.74; H, 3.91; N, 11.80;Cl, 5.98; S, 5.40; M, 9.47. FT-IR (KBr, ν(OH); 3129m, δ(OH); 1320m, 666m, ν(C-O); 1296m, ν(C=S); 1226m, ν(C-S); 1443, ν(N=N);1491m, ν(C=N); 1626sh, ν(N-H); 3050s, ν(M-O); 545w, ν(M-N); 448w, ν(M-S);413w. μ_{eff} (BM) Diam; Λ_m (Ω^{-1} mol^{-1} cm^2) 106.7.

$[Mn(H_2L)_2(H_2O)_2].Cl_2$; yield 86%; m.p.260 °C; white solid. Anal. Calc. for $C_{60}H_{46}Cl_2MnN_{10}O_2S_2$(%): C, 63.89; H, 4.17; N, 12.47; Cl, 6.32; S, 5.73; M, 4.92.Found (%): C, 63.83; H, 4.11; N,12.41;Cl, 6.28; S,5.68 M;4.87. FT-IR (KBr, ν(OH); 3137m, δ(OH); 1362m, 667m, ν(C-O); 1298m, ν(C=S); 1235m, ν(C-S); 1459m, ν(N=N);1484m, ν(C=N); 1626sh, ν(N-H); 3052s, ν(M-O); 544w, ν(M-N); 448w, ν(M-S);410w. μ_{eff} (BM) 5.324; Λ_m (Ω^{-1} mol^{-1} cm^2) 105.7.

3.5. Spectrophotometric studies

Within the wavelength range from 200 to 700 nm for 1×10^{-4} M solutions of the free ligand and metal complexes, the absorption spectra were recorded.

3.6. Molecular docking

Both Auto Dock 4.2 and docking calculations with the ligand (designed drug) atoms subjected to Gasteiger partial charges were used. Calculations of the ligand-protein pattern were done. Clarifying rotatable bonds and connecting nonpolar hydrogen atoms. After the introduction of fundamental hydrogen atoms, Kollmanunified atom type charges and solvation parameters were applied using the Auto Dock tools [45–47].The Auto Dock parameter set and the distance-dependent dielectric functions were used to calculate the van der Waals and electrostatic terms, respectively. The Lamarckian genetic algorithm and the Solis and Wets local search technique were used to simulate docking. The initial position, orientation, and torsions of the ligand molecule were also defined.

 doi:10.20944/preprints202310.1652.v1

3.7. Biological activity

Agar disc diffusion method can be used to predict therapeutic outcomes using antimicrobial susceptibility testing for novel compounds as antimicrobials [48]. The evaluated substances were examined for their in vitro antibacterial activity using the agar disc diffusion assay, which, in accordance with the Clinical and Laboratory Standards Institute (CLSI), is one of the most widely, used manual AST procedures in clinical microbiology laboratories. Simpleness, reproducibility, ease of customizing antimicrobial discs, and the ability to utilise the test as a screening test for a variety of bacterial isolates are the key benefits. Mueller-Hinton agar plates are inoculated with a standardized inoculums of the tested bacterial species; Bacillus subtilis (ATCC 6633), Staphylococcus aureus (ATCC 6538), and Escherichia coli (ATCC 8739), as G-positive but Escherichia coli and Pseudomonas aeruginosa (ATCC 9027), as G-negative bacterial standard isolates *Aspergillus nigar* and *C. albicans* are examples of fungi creatures. Each disc was placed on the inoculated agar surface using commercially prepared paper discs (about 6 mm in diameter) impregnated with 10 µl of the required concentration of the tested drug. According to appropriate guidelines, agar plates are incubated for 16–24 hours at 35–37°C (CLSI2018a; EUCAST 2019b).The diameter of each compound-impregnated disc is then measured in millimeters, and the result also takes into account the diameter of the clear inhibition zones surrounding each disc. This is done by hand while holding a ruler against the back of the inverted agar plate [49]. Gentamycin, ampicillin, and nystatin were utilized as reference drugs standard for Gram-positive, Gram-negative, and fungal antibacterial activities, whereas DMSO was employed as negative control. The outcomes of all the inoculation plates were examined in a table after 35°C incubation. The MIC values have an inverse relationship with the inhibitory zone. The lower the antimicrobial drug concentration needed to stop the growth, the greater the zone of growth inhibition. However, it is important to consider a compound's diffusibility [49].

3.8. Computational methodology

The ideal structural geometry of hydrazones ligand was computed with Gaussian09 software utilizing the Ground state, DFT, B3LYP, and 3-21G. The molecular visualization programme Gauss View was used to display Gaussian files [50]. The HOMO-LUMO energies used to compute the DFT/B3LYP quantum chemical parameters were in agreement with the numerical pattern depicted in the view of compounds in the gas phase. Important bond lengths, bond angles, dihedral angles, charges, and excitation energy for coordinating groups were also computed in optimised structures.

4. Conclusion

The ligand was investigated physic chemically, spectroscopically, and thermally, as well as its complexes with transition metals. The compounds' octahedral geometry was identified using spectroscopic and elemental data. The measured molar conductivity values indicate that the counter chloride ions were found outside of the coordination sphere. Additionally, after examining each molecule's antibacterial characteristics, the $[Co(HL)(H_2O)_2]Cl_2$ and $[Ni(HL)(H_2O)_2]Cl_2$ combination was shown to be the most effective antibacterial compound. A wide variety of ligand activity toward various types of proteins with modest binding was found in the findings of ligand docking studies.

Supplementary Materials: The following supporting information can be downloaded at the website of this paper posted on Preprints.org.

References

1. Muhammad, M.T., Ghouri, N., Khan, K.M., Choudhary, M.I., Perveen, S. Synthesis of Thiocarbohydrazones and Evaluation of their in vitro Antileishmanial Activity. Medicinal Chemistry. 2018, 14, 725-32.
2. Alzahrani, A.Y., Ammar, Y.A., Abu-Elghait, M., Salem, M.A., Assiri, M.A., Ali, T.E., et al. Development of novel indolin-2-one derivative incorporating thiazole moiety as DHFR and quorum sensing inhibitors:

Synthesis, antimicrobial, and antibiofilm activities with molecular modelling study. Bioorganic Chemistry. 2022, 119, 105571.

3. Ragab, A., Ammar, Y.A., Ezzat, A., Mahmoud, A.M., Mohamed, M.B.I., Abdou, S., et al. Synthesis, characterization, thermal properties, antimicrobial evaluation, ADMET study, and molecular docking simulation of new mono Cu (II) and Zn (II) complexes with 2-oxoindole derivatives. Computers in Biology and Medicine. 2022, 145, 105473.
4. Divya, K., Pinto, G.M., Pinto, A.F. Application of metal complexes of Schiff bases as an antimicrobial drug: a review of recent works. Int. J. Curr. Pharm. Res. 2017, 9, 27-30.
5. Malik, M.A., Dar, O.A., Gull, P., Wani, M.Y., Hashmi, A.A. Heterocyclic Schiff base transition metal complexes in antimicrobial and anticancer chemotherapy. MedChemComm. 2018, 9, 409-36.
6. Santacruz, M.C.S., Fabiani, M., Castro, E.F., Cavallaro, L.V., Finkielsztein, L.M. Synthesis, antiviral evaluation and molecular docking studies of N4-aryl substituted/unsubstituted thiosemicarbazones derived from 1-indanones as potent anti-bovine viral diarrhea virus agents. Bioorganic & Medicinal Chemistry. 2017, 25, 4055-63.
7. Sabri, M.S.M., Wei, O.C., Fei, Y.M. Synthesis, characterisation and vasolidation properties of indanone-based chalcones. Journal of Physical Science. 2018, 29, 99-106.
8. Medvedev, A., Buneeva, O., Kopylov, A., Tikhonova, O., Medvedeva, M., Nerobkova, L., et al. Brain mitochondrial subproteome of Rpn10-binding proteins and its changes induced by the neurotoxin MPTP and the neuroprotector isatin. Biochemistry (Moscow). 2017, 82, 330-9.
9. Guo, H. Isatin derivatives and their anti-bacterial activities. European Journal of Medicinal Chemistry. 2019, 164, 678-88.
10. Pradeep, S.D., Gopalakrishnan, A.K., Manoharan, D.K., Soumya, R.S., Gopalan, R.K., Mohanan, P.V. Isatin derived novel Schiff bases: An efficient pharmacophore for versatile biological applications. Journal of Molecular Structure. 2023, 1271, 134121.
11. Zayed, E.M., Mohamed, G.G., Hindy, A.M. Transition metal complexes of novel Schiff base: Synthesis, spectroscopic characterization, and in vitro antimicrobial activity of complexes. Journal of Thermal Analysis and Calorimetry. 2015, 120, 893-903.
12. Ramadan, R.M., Al-Nasr, A.K.A., Noureldeen, A.F. Synthesis, spectroscopic studies, antimicrobial activities and antitumor of a new monodentate V-shaped Schiff base and its transition metal complexes. Spectrochimica Acta Part A: Molecular and Biomolecular Spectroscopy. 2014, 132, 417-22.
13. Matin, S., Khojasteh, R. Synthesis, characterization, and antibacterial activities of Cr (III), Co (III), Ni (II), and Mn (III) complexes of heptadentate Schiff base ligand derived from tris (2-aminoethyl) amine. Russian Journal of General Chemistry. 2015, 85, 1763-7.
14. Rajee, A.O., Babamale, H.F., Lawal, A., Aliyu, A.A., Osunniran, W.A., Sheriff, A.O., et al. Mn (II), Co (II), Ni (II), and Cu (II) complexes of amino acid derived Schiff base ligand: Synthesis, characterization and in-vitro antibacterial investigations. Bulletin of the Chemical Society of Ethiopia. 2021, 35, 97-106.
15. Abdel-Rhman, M.H., El-Asmy, A.A., Ibrahim, R., Hosny, N.M. New Schiff base ligand and some of its coordination compounds: Synthesis, spectral, molecular modeling and biological studies. Journal of Molecular Structure. 2023, 1279, 135023.
16. Chang, C., Chen, W., Chen, Y., Chen, Y., Chen, Y., Ding, F., et al. Recent progress on two-dimensional materials. Acta Phys. Chim. Sin. 2021, 37, 2108017.
17. Mahadevi, P., Sumathi, S., Metha, A., Singh, J. Synthesis, spectral, antioxidant, in vitro cytotoxicity activity and thermal analysis of Schiff base metal complexes with 2, 2′-Bipyridine-4, 4′-dicarboxylic acid as co-ligand. Journal of Molecular Structure. 2022, 1268, 133669.
18. Zayed, E.M., Mohamed, G.G., Hassan, W.M., Elkholy, A.K., Moustafa, H. Spectroscopic, thermal, biological activity, molecular docking and density functional theoretical investigation of novel bis Schiff base complexes. Applied Organometallic Chemistry. 2018, 32, e4375.
19. Yadav, M., Sharma, S., Devi, J. Designing, spectroscopic characterization, biological screening and antioxidant activity of mononuclear transition metal complexes of bidentate Schiff base hydrazones. Journal of Chemical Sciences. 2021, 133, 1-22.
20. Radha, V.P., Chitra, S., Jonekirubavathi, S., Chung, I.-M., Kim, S.-H., Prabakaran, M. Transition metal complexes of novel binuclear Schiff base derived from 3, 3′-diaminobenzidine: synthesis, characterization, thermal behavior, DFT, antimicrobial and molecular docking studies. Journal of Coordination Chemistry. 2020, 73, 1009-27.

21. Farag, A.M., Sokker, H.H., Zayed, E.M., Eldien, F.A.N., Abd Alrahman, N.M. Removal of hazardous pollutants using bifunctional hydrogel obtained from modified starch by grafting copolymerization. International journal of biological macromolecules. 2018, 120, 2188-99.
22. Manan, M.A.F.A., Mohammat, M.F. Synthesis, structural studies and antimicrobial evaluation of nickel (II) bis-complex of Schiff base of S-benzyldithiocarbazate. Trends in Sciences. 2022, 19, 1500-.
23. Pedro, K.C.N.R., Ferreira, I.E.P., Henriques, C.A., Langone, M.A.P. Enzymatic fatty acid ethyl esters synthesis using acid soybean oil and liquid lipase formulation. Chemical Engineering Communications. 2020, 207, 43-55.
24. Zhang, C., Xu, C., Gao, X., Yao, Q. Platinum-based drugs for cancer therapy and anti-tumor strategies. Theranostics. 2022, 12, 2115.
25. Sudha, A. Evaluation of characterization, biological and computational studies of new Schiff base ligand and some metal (II) complexes. Inorganica Chimica Acta. 2022, 534, 120817.
26. Zayed, E.M., Zayed, M.A., Radwan, M.A., Alminderej, F.M. Synthesis, characterization, antimicrobial, and docking study of novel 1-(furanyl)-3-(pyrrolyl) propenone-based ligand and its chelates of 3d-transition metal ions. Applied Organometallic Chemistry. 2022, 36, e6489.
27. Eldeken, G.A., El-Samahy, F.A., Zayed, E.M., Osman, F.H., Elgemeie, G.E. Synthesis, biological activities and molecular docking analysis of a novel series of 11H-indeno [1, 2-b] quinoxalin-11-one derivatives. Journal of Molecular Structure. 2022, 1261, 132929.
28. Zayed, E.M., Zayed, M.A., Hindy, A.M., Mohamed, G.G. Coordination behaviour and biological activity studies involving theoretical docking of bis-Schiff base ligand and some of its transition metal complexes. Applied Organometallic Chemistry. 2018, 32, e4603.
29. Çelik, F., Ünver, Y. 1, 2, 4-Triazole derivative containing thiophen ring: Comparison of theoretical IR and NMR data with experimental. Journal of the Indian Chemical Society. 2022, 99, 100455.
30. Zayed, E.M., El-Samahy, F.A., Mohamed, G.G. Structural, spectroscopic, molecular docking, thermal and DFT studies on metal complexes of bidentate orthoquinone ligand. Applied Organometallic Chemistry. 2019, 33, e5065.
31. Ahmed, Y.M., Mohamed, G.G. New Tin (IV) Schiff base complexes: synthesis, characterization and antibacterial investigation, docking and theoretical studies. Inorganic Chemistry Communications. 2022, 144, 109864.
32. Zayed, E.M., Mohamed, G.G., Abd El Salam, H.A. Ni (II), Co (II), Fe (III), and Zn (II) mixed ligand complexes of indoline-dione and naphthalene-dione: Synthesis, characterization, thermal, antimicrobial, and molecular modeling studies. Inorganic Chemistry Communications. 2023, 147, 110276.
33. Kumar, S., Devi, J., Dubey, A., Kumar, D., Jindal, D.K., Asija, S., et al. Co (II), Ni (II), Cu (II) and Zn (II) complexes of Schiff base ligands: Synthesis, characterization, DFT, in vitro antimicrobial activity and molecular docking studies. Research on Chemical Intermediates. 2023, 49, 939-65.
34. Zayed, E.M., Zayed, M.A., Abd El Salam, H.A., Nawwar, G.A. Synthesis, structural characterization, density functional theory (B3LYP) calculations, thermal behaviour, docking and antimicrobial activity of 4-amino-5-(heptadec-8-en-1-yl)-4H-1, 2, 4-triazole-3-thiol and its metal chelates. Applied Organometallic Chemistry. 2018, 32, e4535.
35. Kanagasabapathy, G., Britto, S., Anbazhagan, V. Synthesis, characterization and molecular docking studies of highly functionalized and biologically active derivatives of 2-aminothiazole. Journal of Molecular Structure. 2023, 1275, 134593.
36. Hassaballah, A.I., El-Ziaty, A.K., Ewies, E.F., Zayed, E.M., Mohamed, G.G. Synthesis of pyrimidine ligand and its mononuclear metal (II)/(III) complexes: Spectroscopic characterization, thermal, DFT, molecular docking, antimicrobial and anticancer studies. Inorganic Chemistry Communications. 2023, 155, 110989.
37. Ali, A., Pervaiz, M., Saeed, Z., Younas, U., Bashir, R., Ullah, S., et al. Synthesis and biological evaluation of 4-dimethylaminobenzaldehyde derivatives of Schiff bases metal complexes: A review. Inorganic Chemistry Communications. 2022, 145, 109903.
38. Moustafa, G., Sabry, E., Zayed, E.M., Mohamed, G.G. Structural characterization, spectroscopic studies, and molecular docking studies on metal complexes of new hexadentate cyclic peptide ligand. Applied Organometallic Chemistry. 2022, 36, e6515.
39. Gopichand, K., Mahipal, V., Rao, N.N., Ganai, A.M., Rao, P.V. Co (II), Ni (II), Cu (II), and Zn (II) complexes with Benzothiazole Schiff base ligand: Preparation, Spectral Characterization, DNA Binding, and In Vitro Cytotoxic Activities. Results in Chemistry. 2023, 5, 100868.

40. Zayed, E.M., Abd ElSallam, H.A., Fathala, M.I., Sroor, F.M. Naphthalene-1, 2-dione and indoline-2, 3-dione as Convenient Ligands to Prepare Mixed Ligand Complexes of Mn, Cu And Cd: Synthesis, Spectroscopic Characterization, DFT Studyand Antibacterial Activity. ChemistrySelect. 2023, 8, e202300145.
41. Abd El Salam, H.A., Mohamed, G.G., Zayed, E.M. Synthesis, spectroscopic characterization, biological application and molecular docking studies of some transition metal complexes of isophthalamide ligand. Journal of Molecular Structure. 2023, 1273, 134231.
42. Abd El Salam, H.A., Moustafa, G., Zayed, E.M., Mohamed, G.G. Isophthaloylbis (Azanediyl) Dipeptide Ligand and Its Complexes: Structural Study, Spectroscopic, Molecular Orbital, Molecular Docking, and Biological Activity Properties. Polycyclic Aromatic Compounds. 2022, 1-23.
43. Benabid, W., Ouari, K., Bendia, S., Bourzami, R., Ali, M.A. Crystal structure, spectroscopic studies, DFT calculations, cyclic voltammetry and biological activity of a copper (II) Schiff base complex. Journal of Molecular Structure. 2020, 1203, 127313.
44. Zayed, E.M., Ewies, E.F., Hassaballah, A.I., Mohamed, G.G. Synthesis, characterization, DFT, docking, antimicrobial and thermal study of pyrimidine-carbonitrile ligand and its metal complexes. Journal of Molecular Structure. 2023, 1284, 135396.
45. Zayed, E.M., Zayed, M. Synthesis of novel Schiff's bases of highly potential biological activities and their structure investigation. Spectrochimica Acta Part A: Molecular and Biomolecular Spectroscopy. 2015, 143, 81-90.
46. Abd El Salam, H.A., Fathy, U., Zayed, E.M., El Shehry, M.F., Ahmed E. Gouda, a. Design, Synthesis, Cytotoxic Activity and Molecular Docking Studies of Naphthyl Pyrazolyl Thiazole Derivatives as Anticancer Agents. ChemistrySelect. 2023, 8, e202203956.
47. Zayed, E.M., Zayed, M., El-Desawy, M. Preparation and structure investigation of novel Schiff bases using spectroscopic, thermal analyses and molecular orbital calculations and studying their biological activities. Spectrochimica Acta Part A: Molecular and Biomolecular Spectroscopy. 2015, 134, 155-64.
48. Reiss, A., Cioateră, N., Dăbuleanu, I., Chifiriuc, M.C., Amzoiu, E., Rotaru, P. New metal (II) complexes with ceftazidime Schiff base. Journal of Thermal Analysis & Calorimetry. 2018, 131.
49. Olar, R., Badea, M., Ferbinteanu, M., Stanica, N., Alan, I. Spectral, magnetic and thermal characterization of new Ni (II), Cu (II), Zn (II) and Cd (II) complexes with a bischelate Schiff base. Journal of Thermal Analysis and Calorimetry. 2017, 127, 709-19.
50. Zarafu, I., Olar, R., Chifiriuc, M.C., Bleotu, C., Ioniţă, P., Mulţescu, M., et al. Synthesis, thermal, spectral, antimicrobial and cytotoxicity profile of the Schiff bases bearing pyrazolone moiety and their Cu (II) complexes. Journal of Thermal Analysis and Calorimetry. 2018, 134, 1851-61.